Proceedings World Geothermal Congress 2020+1
Reykjavik, Iceland, April - October 2021

Resistivity Structure of Shalla-Abayata Geothermal Field, Southwest Ethiopia, Using Magnetotelluric Data Inversion

Yosef K. KETO[1] and Hakim SAIBI[2]

[1]Geological Survey of Ethiopia, Addis Ababa, Ethiopia.

E-mail: kebedeyosef4@gmail.com / yosef@mine.kyushu-u.ac.jp

[2]Geology Department, College of Science, UAEU, Al-Ain, UAE

E-mail: hakim.saibi@uaeu.ac.ae

Keywords: dimensionality analysis, magnetotelluric inversion, resistivity structure, Shalla-Abayta, geothermal field, Ethiopia.

ABSTRACT

The Main Ethiopian Rift (MER) constitutes an area characterized by active extensional tectonics with the two main fault systems in the MER, NE-SW trending and NNE-SSW trending faults, which define the Wonji fault belt (WFB). In this study, 15 magnetotelluric (MT) stations were collected with period range from 0.003s to 1000s. The MT stations where located south of Lake Abayata and Langano and northeast of Lake Shalla, set close to the eastern escarpment of the rift along the WFB. The main objective of this study is to understand the nature of the MT data and to apply inversion to detect and delineate the geothermal resource and locate exploitable reservoir.

The dimensionality analysis, ellipticity and skew, of the MT soundings has 2D/1D character. Dimensionality increases at depth. 2D and 3D inversions were done to interpret the MT data as a result of the dimensionality analysis. For the inversions, the MT data were rotated to 35^0 using the tipper strike direction result and fault directions to fit the data in the polarization.

The phase tensor pseudo-section shows low resistivity beneath a thin layer of high resistivity at the surface and the ellipses look circular showing 2D/1D character. The resistivity increases with depth and the ellipses indicate 3D character. The Phase tensor pseudo-section result correlated with the resistivity distribution of the inversion results.

The 2D and 3D inversion result have low resistivity (1-10 ohm-meter) and 1.2 km depth benth the top surface thin layer high resistive (tens to hundreds ohm-meter) which is fresh volcanic overburden unaffected by alteration. Most probably, the low resistive layer is the clay cap rock and shallow depth reservoir in the sedimentary formation which is conductive hydrothermal mineral alteration smectite and illite. Below the interpreted clay cap and shallow depth reservoir, resistivity values tend to increase at interval 20-100-ohm meter which is interpreted as zone of reservoir due to the formation of high temperature mineral chlorite-epidote starting from 2 km depth. The result corresponds very well with the conceptual model of a high enthalpy geothermal system comprising a resistive up-flow region at depth overlain by a conductive clay cap.

1. INTRODUCTION

Electrical power generation from geothermal energy is evident when connected to the electrical grid or on remote locations with insufficient power supply with a high energy demand or areas where other energy sources are scarce or expensive. Geothermal energy is exploited for electrical power generation or for direct heat applications. Ethiopia is a developing country and energy is the main accelerator for the development of the country. Shalla-Abayata geothermal field is located in the central part of the Main Ethiopian Rift (MER) system enclosed by Lake Abayata and Langano in the north and Lake Shalla in the south west (Fig.1).

The Main Ethiopian Rift constitutes an area characterized by active extensional tectonics and the two main fault systems have been identified in the area, NE-SW trending fault system which characterizes the rift margins, and a NNE-SSW trending fault system, the Wonji fault belt (WFB) (Fig.1). The WFB is active since the early quaternary and it is the youngest part of the MER (Mohr, 1967, Kurtz et al., 2007; ELC, 2015). The study area is near Langano-Aluto geothermal field and the results of the surface exploration and drilling in Aluto-Langano area indicated the existence of a high-enthalpy geothermal system with temperatures greater than 300 ^{0}C (Gebregzabher, 1986; Gianelli and Teklemariam, 1993).

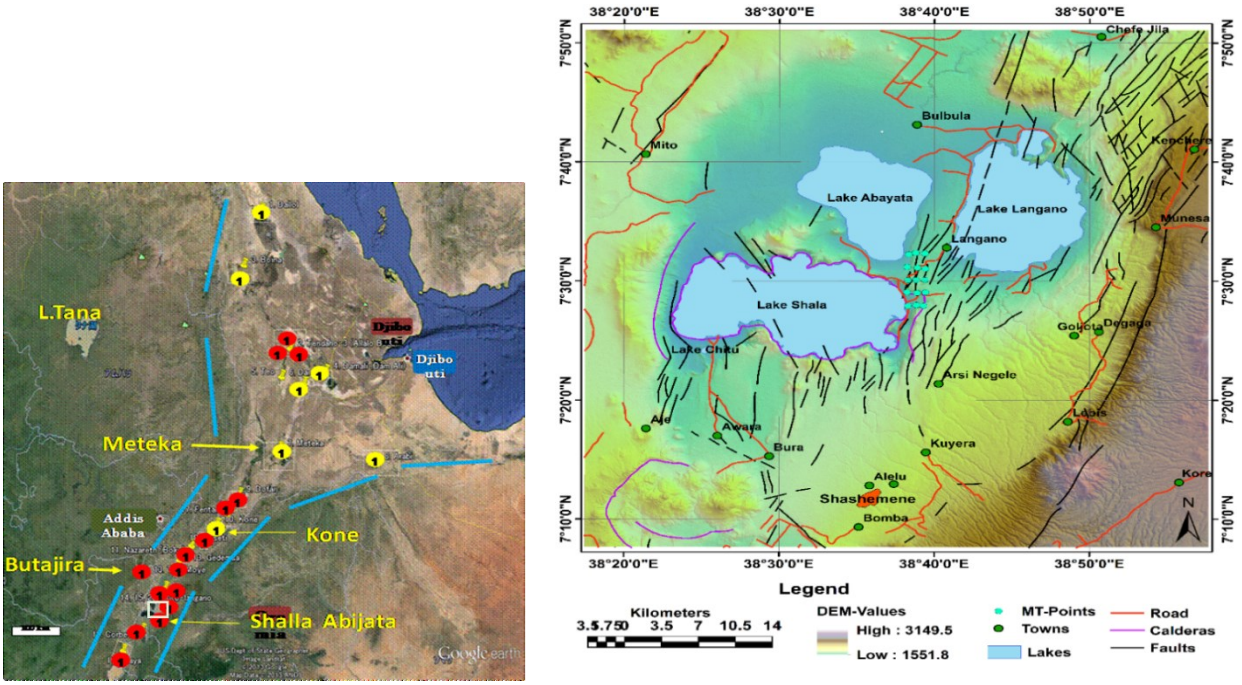

Figure 1: Location map of the main Ethiopian Rift System and Shalla-Abayata geothermal field located south of the capital city Addis Ababa (left). Physiographic map of the study area and the MT stations surrounded by lakes of Shalla, Abayata and Langano, close to Langano geothermal field (right).

In the study area 15 MT stations were collected by the Geological Survey of Ethiopia to help determine a conceptual model for the study area, and to delineate the subsurface geological structure and geothermal reservoir. The MT data were processed using the robust processing program SSMT2000 (Phoenix Geophysics Ltd) similar to Egbert, 1997; Smirnov, 2003. The cross-powers were then graphically edited by the MT editor program to remove the noisy data points and generate "smooth" curves for both phase and apparent resistivity. Almost all sounding data have good quality and can be used for interpretation from period of 0.003 s to 1000 s.

The magnetotelluric (MT) method makes use of natural electromagnetic (EM) fields, from magnetospheric and ionospheric currents, measured on the surface of the Earth to study the subsurface electrical resistivity (Chave and Jones, 2012). The geoelectrical model of the subsurface formations is obtained by inverting the observed impedance data, which are the ratio of the electric and magnetic fields.

The deployment of the magnetotelluric method during geothermal exploration in convection-dominated play types is widespread and common practice in the geothermal industry. The characteristic electrical resistivity response of volcanic geothermal systems with a conductive resistive clay cap of alteration clay minerals overlying a more electrically resistive geothermal reservoir, as shown in Figure 2, is an excellent setting for a magnetotelluric survey (Cumming, 2009; Pellerin et al., 1996). In reality, the resistivity response of a volcanic geothermal play type is not as straight-forward as in this theoretical example.

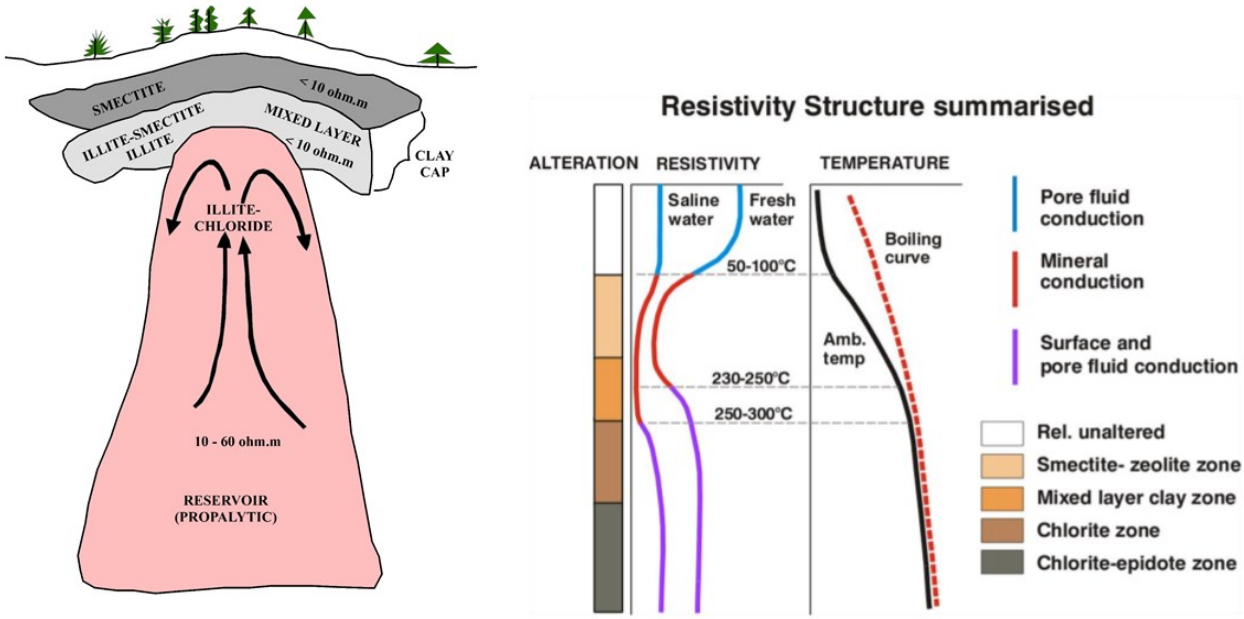

Figure 2: Generalized electrical resistivity structure of a volcanic geothermal system. Smectite and illite are clay alteration minerals redrawn from Pellerin et al. (1996). The resistivity structure consists of resistive shallow layer, conductive clay cap, generally resistive reservoir and heat source. Black arrows describe the fluid flow (left). Generalized resistivity structure of a basaltic geothermal system from Flóvenz et al. (2005). Plotted as a function of depth are from left to right, the clay alteration, the electrical resistivity of saline and fresh water and the ambient and boiling temperatures (right).

In this study 2D and 3D inversion models of the rotationally invariant of impedance tensor of MT data were done using Occam for 2D (Constable et al., 1987) and ModEM program for 3D (Egbert and Kelbert, 2012). The results of MT data in the study area reveal three main resistivity structures at different depths. The first shallow layer structure is surface resistive fresh volcanic overburden unaffected by alteration and lacustrine sediment. The second structure is a low resistivity structure conductive clay cap and shallow depth reservoir, probably argillic hydrothermal alteration zone with temperature below 200 ^{0}C (Teklemariam *et al.*1996). The last structure is a resistive structure of a basaltic geothermal system, chlorite zone. The EW section of Aluto-Langano geothermal field inversion result taken from Gianelli & Teklemariam (1993) shows the isotherm pattern as interpreted from interpolated well data and the result agrees with the conceptual model of a high enthalpy geothermal reservoir. By gravity data analysis Saibi et al. (2012) could clearly identify the WFB as highly fractured area intersecting the volcanic complex at the location of the productive wells LA3 and LA6.

2. GEOLOGICAL AND TECTONIC SETTING

Uplift, doming and eventual rupture of the Afro-Arabian region resulted in the formation of the East African Rift system oriented in NE-SW and NNE-SSW directions. It is now generally accepted that the initial sagging of the main Ethiopian Rift began around 15 to 14 million years (Ma) ago. An important event in the rift development took place around 10 my ago (Kazmin et al., 1978) by faulting of the pre-rift volcanic succession during Oligocene-Miocene age. Deposits ranging from Miocene-Pliocene to Holocene cover the floor of the rift valley (Kazimin et al., 1978). A thick succession of stratoid silicics, ignimbrites, unwelded tuffs, ash flows, rhyolite and trachyte flows and domes form large part of the rift floor and also outcrops on the rift escarpments and adjacent plateau margins referred as Nazreth Group. In the rift floor, the Nazreth Group is overlain by a sequence of flood basalts of Pliocene age referred as Bofa Basalts (Fig. 3).

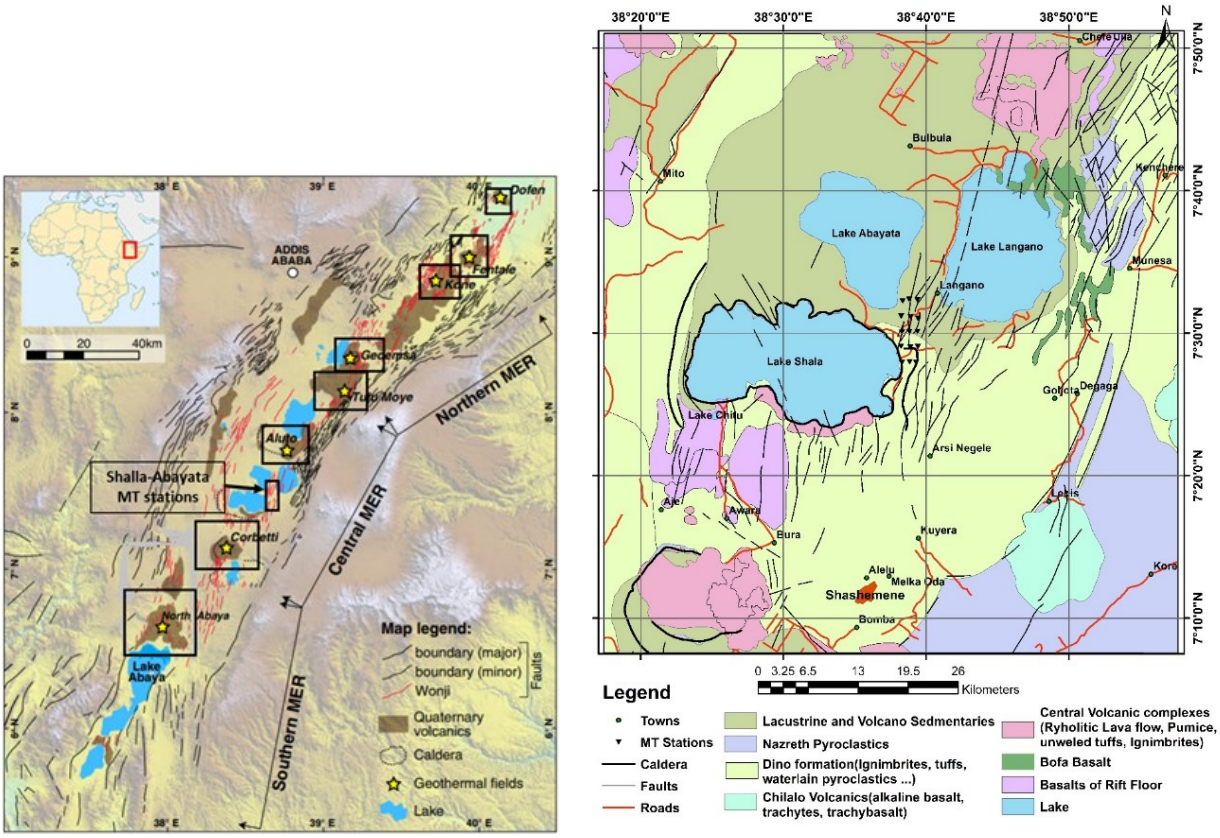

Figure 3: Tectonic setting of the Main Ethiopian Rift (MER)(left) and Geological and structural map of Shalla, Abayata and Langano lake area(right).

An intense tectonic event occurred in the Pleistocene-Holocene in the main Ethiopian Rift related to the Wonji Fault (Mohr, 1967). With the formation of the Wonji Fault Belt, tectonic movements and volcanic activity produced step-like structures and associated volcanic activity, represented by ignimbrites, basalts and unwedded pyroclastics. The fault zone is straddled by central volcanoes disposed along the axial zone of the Wonji Fault Belt. The main products were rhyolite, trachyte lava flows, pumice, unwedded tuffs, obsidians and pitch stones. The products of the Wonji fault are referred as Wonji Group (Kazmin at al., 1978 and others). Another type of volcanic activity in Wonji Fault Belt was the eruption from fissures of Pleistocene to Recent basalt lava flows (Fig. 3). The basalts are controlled by extensional fractures and commonly characterized by fresh aa surface. Chains of scorraceous cones follow the lines of fractures. These basalts are mostly found in the rift floor; south of lake Ziway and lake Shalla. Recent flows in many cases follow pre-existing topographic low relief areas. Although the development of the rift was dominated by volcanic activity, sedimentation also occurred. Wonji Group rocks are intimately associated with lacustrine sediments related to the ancestral lake in the rift floor in the Pleistocene-Holocene times.

Most part of the rift floor especially the surrounding area of Lake Langano, Ziway and Awassa are covered by Pleistocene-Holocene age lacustrine sediments. They were deposited in a huge lake whose level thousands years before was much higher than at the present. The sediments are mainly represented by sand and silt. They are intercalated with volcanic, mainly ashes and tuffs which in places are extensively developed. Micro-organic deposits (diatomite) occur associated with these lake sediments.

3. DIMENSIONALITY AND DIRECTIONALITY ANALYSIS

The MT transfer functions allow the analysis of the dimensional and directional properties of the subsurface resistivity of the research area. Dimensionality and directionality analysis examines how well the data fit the assumed model, and extracts the best fitting. The information of the dimensionality of the area confirms selection of proper tools to invert and interpret the MT data. The phase tensor, unaffected by galvanic distortion, provided a practical tool to easily obtain information about the dimensionality (Bibby et al., 2005). In this study, some techniques that used to determine the dimensionality and directionality of the electrical conductivity structures are Bahr Skew, ellipticity, and strike direction.

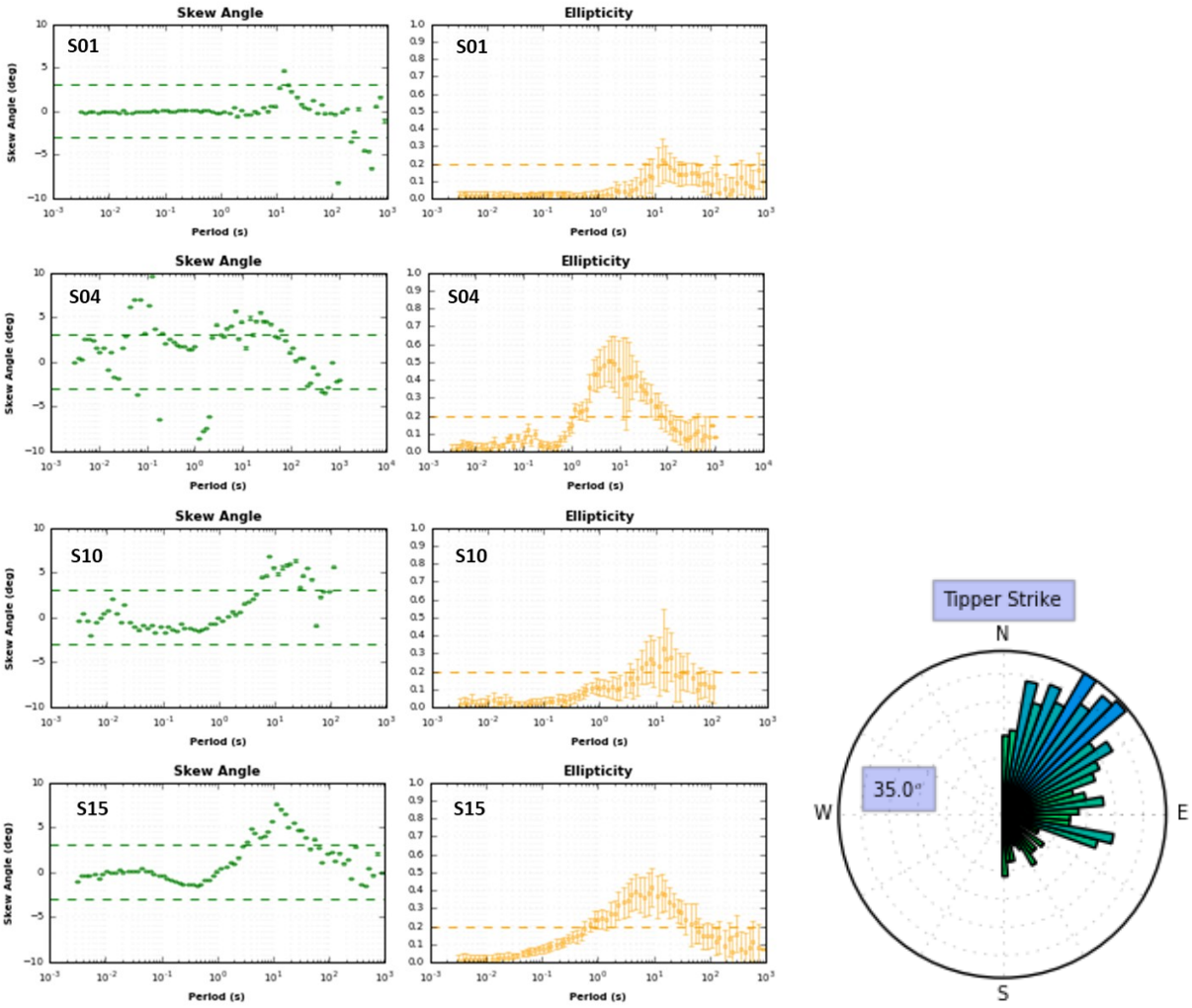

Figure 4: Bahr's phase-sensitive skew and phase ellipticity for some MT stations in the study area (left). The tipper strike direction for all MT stations period (right).

Bahr skew (BS) is a measure of the local 3D distortion of regional 2D fields based on impedance phase, rather than on impedance magnitudes, which is the conventional definition of skew (Vozoff, 1972). According to Bahr's (1988) recommendation, the regional 2D indicator (3D/2D skew) should be below 3 for regional 2D structures. Figure 4 shows the Bahr skew at some stations and most of the skew values are smaller than 3, showing 2D/1D structure (Bahr, 1988). The 3D effect can be clearly seen around the period of 10 s.

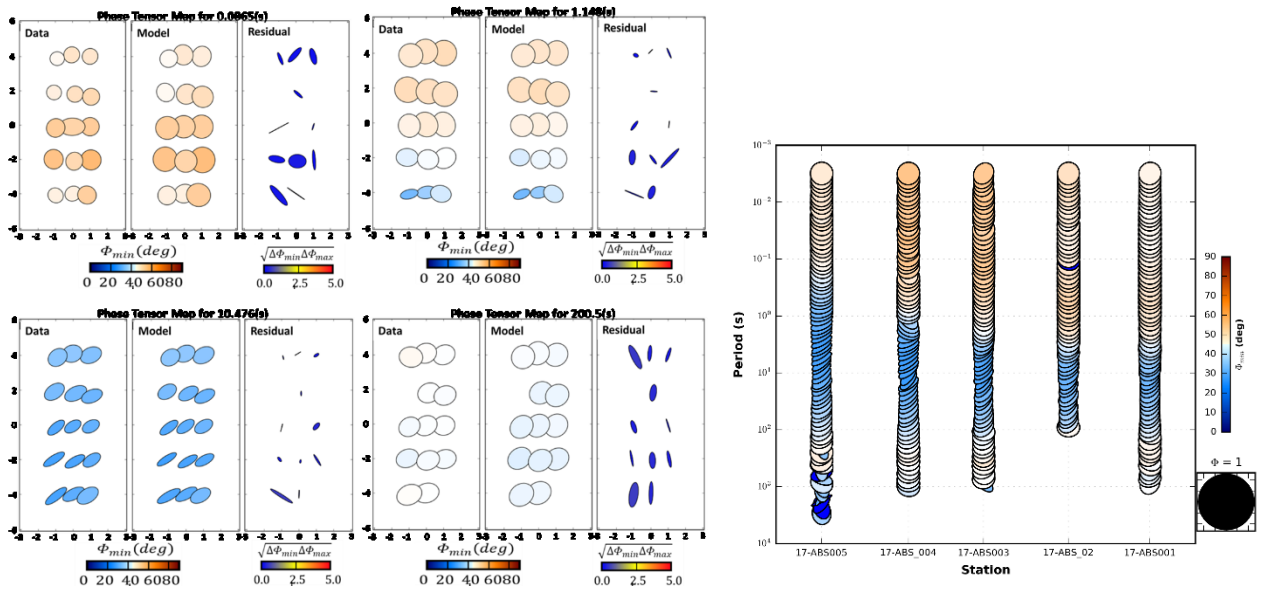

Figure 5: Phase tensor ellipses for selected periods of 0.08 s, 1.14 s, 10.47 s and 200.7 s. The Data, Calculated and residual phase tensor ellipses from 3D inversion for respective periods. The data and model ellipses are colored by the minimum principal phase. The residual ellipses are colored by percentage of the geometric mean of changes in maximum and minimum phases of observed and calculated phase tensors. The small size of ellipse indicates that the misfit is small (left). Elliptical representation of phase tensor pseudo-section (right).

The phase tensor can be represented graphically as ellipses, providing information about the dimensionality of the geoelectrical structure (Caldwell et al., 2004). The long axis of the phase tensor (Φmax) aligns in the direction of preferred current flow (i.e. geoelectric strike direction Fig. 4 and Fig. 5) with a 90º ambiguity and reflects lateral variation of the subsurface structures at different depths (Hamilton et al., 2006; Caldwell et al., 2004). In Figures 4 and 5, at about 10 s, the phase tensors show more elliptical along the strike and the ellipticity values are greater than 0.2. Between 0.009 s to 1 s and below 300 s the ellipse has no preferred direction of current flow (Fig. 5), the phase tensor can be represented as a circle, probably representing 2D/1D structure (Caldwell et al., 2004). The minimum principal phase color values are used to indicate dimensionality (Fig. 5). Values exceeding 45° indicate a decrease of resistivity with depth showing the low resistivity due to alteration minerals between 0.009 s to 1 s and below 300 s. Whereas values less than 45° indicate an increase in resistivity with depth showing the high resistivity around 10 s. This can be interpreted with the formation of secondary minerals like chlorite and epidote. The invariant of the MT data tipper or induction arrow (Wiese, 1962; Parkinson, 1959) show that the regional strike direction is N 35º E direction (Fig. 4). This result correlated with the geology of the study area. The impedance tensor must be rotated to a proper geologic strike direction prior to further analysis and modelling. The MT data rotated N 35º E depending on the strike direction analysis, to get plausible 2D model. Before doing 3D inversion, it is preferred to do rotation of MT data to geoelectric strike direction if some of the resistivity structure is 2D in nature (Tietze and Ritter, 2013).

4. RESULTS AND DISCUSSION

In order to get 2D and 3D conductivity models of the subsurface, we inverted the MT data in the period range of 0.003-1000 s using the Occam and ModEM codes (Constable et al., 1987; Egbert & Kelbert 2012). The program used Occam code for 2D and ModEM code for 3D. The Occam and ModEM modular system comprises forward and inversion schemes for frequency domain EM geophysical data.

The 3D forward scheme is based on finite differences and the inverse scheme exploits the non-linear conjugate gradient method. For the 3D case, the full impedance tensor was used by setting an error Egbert of 3% for the components inverted. 35 periods were used in a period range from 0.003s to 1000s to create the resistivity model. The final resistivity model grid was 29 (north) × 27 (east) × 36 (vertical not including air) cells with 500 m cell size in the horizontal direction within the station area. Outside the station area, padding cells grow with a scale factor of 1.1. The vertical cells increase in size as a function of depth on a logarithmic scale, with the first cell depth being 30 m.

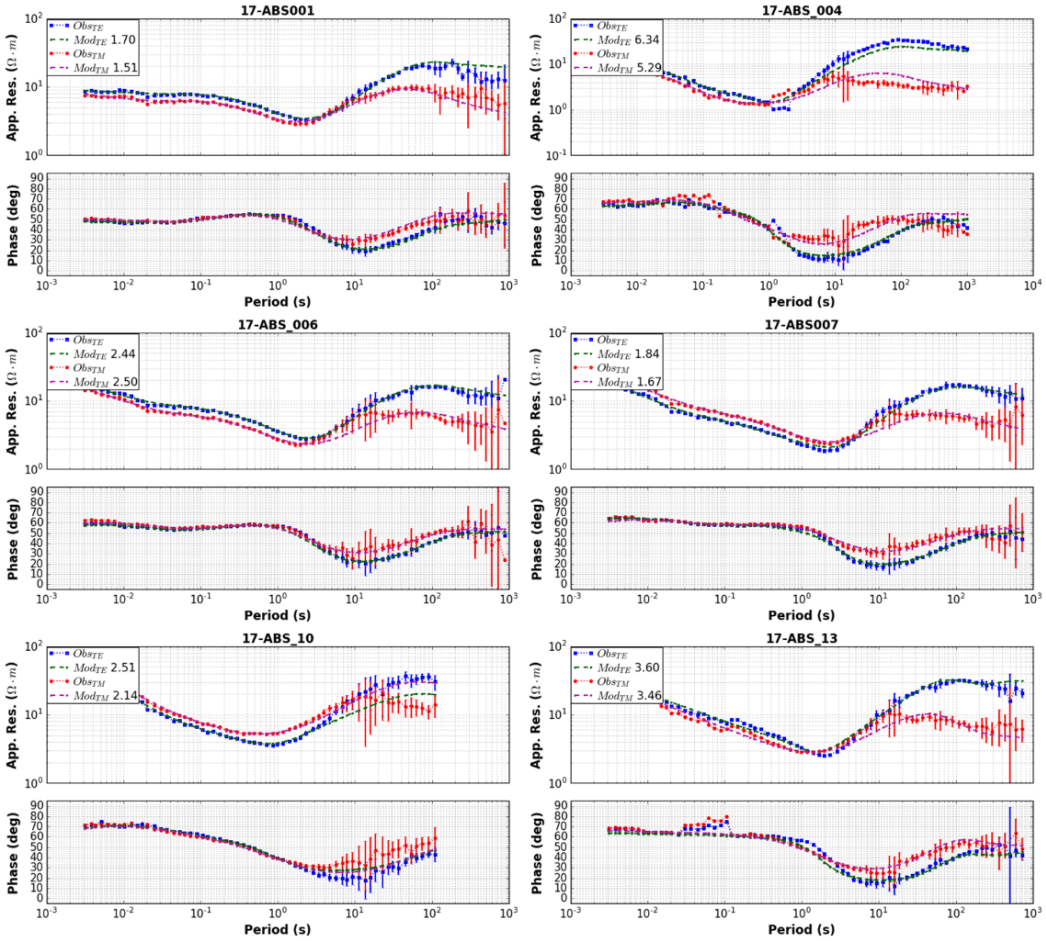

Figure 6: 2D inversion result of the observed and calculated curve fitness for some stations.

Various inversions were performed in order to obtain the smoothest model which could fit the data properly by varying starting resistivity, mesh size and covariance parameters. Many models can fit the data equivalently, prescribing the need for prior geophysical information and model testing due to non-uniqueness. A preferred model was found, for 3D, which has been chosen based on fitness to the data (Fig. 5(left) and 8) and correlation with geophysical data described in geological setting of the study area. The preferred model has a root-mean-square error (RMS) of 2.73 for input data. The model slice maps and the profiles on the final model resulting from 3D inversion are shown in Figure 9 and 10. The data fitness for the 3D model, represented in Figure 8 shows an assessment between measured (dots for apparent resistivity and phase, for both off-diagonal elements of the impedance tensor), and modeled data (the line for apparent resistivity and phase), for some stations from each profile measured.

2D modelling of the MT data along the selected profiles has revealed remarkable confirmation of the subsurface geology with the 3D result. The 2D model and the fitness were shown in Figure 6 and 7.

The dimensionality analysis result of Shalla-Abayata MT shows 2D/1D characters and most of them are conductive from 0.009 s to 1 s and from 300 s to the depth period range according to Swift (1967) and Caldwell et al. (2004), while the result between 1 s to 100 s has 3D character and most are resistive, using Bahr skew and phase tensor following Swift (1967) and Caldwell et al. (2004). The regional strike direction dominated between 1 s to 100 s period ranges, with the NNE-SSW direction (N 35° E) using induction arrow (Caldwell et al., 2004; Wiese, 1962; Parkinson, 1959; Smirnov and Pedersen, 2009). The dimensionality analysis result agrees with the preferred 2D and 3D model of Shalla-Abayata with thin layer of high resistive volcanic rocks on the surface, conductive clay cap alteration and resistive to depth.

The 2D and 3D resistivity distribution of Shalla-Abayata geothermal field model was created using all MT data. The top thin layer of the resultant model is high resistivity with 70 Ωm and interpreted as unaltered volcanic rocks together with dry lacustrine sediment. The next layer is conductive with less than 10 Ωm and this structure is correlated to clay cap and altered volcanic rocks containing geothermal fluids or a zeolite smectite clay alteration mineral zone (> 800 m thickness), acting as both as cap rock and a shallow geothermal reservoir, possibly argillic hydrothermal alteration zone (Teklemariam *et al.*1996). The resistivity increases gradually to 100 Ωm at depth beneath the conductive region due to the formation of high-temperature alteration minerals, particularly chlorite and epidote. This deep resistive body could be identified as zone of up-flow and hottest part of the geothermal field characterized by high temperature and the presence of propyllitic alteration. In this zone, the most common alteration products include chlorite and epidote.

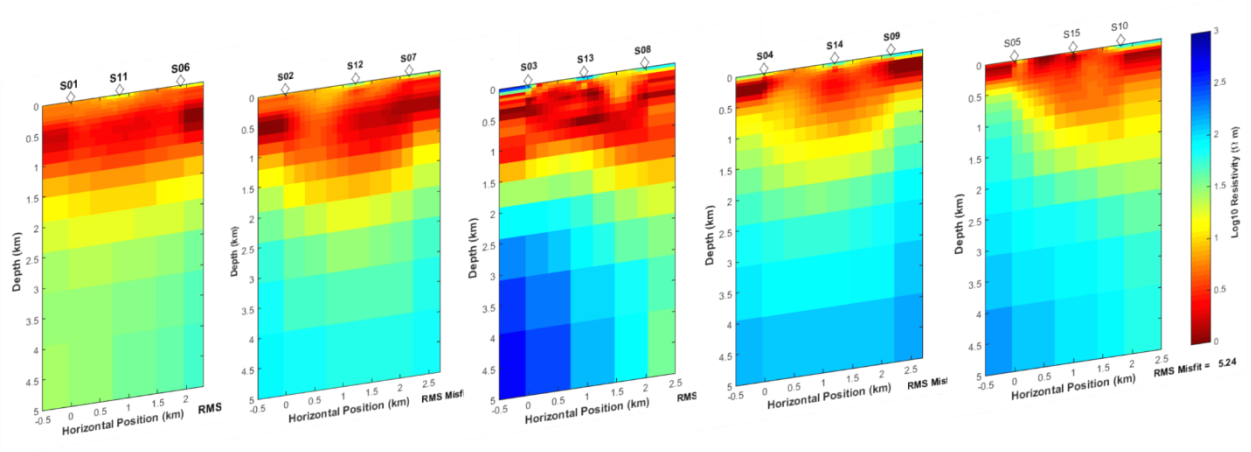

Figure 7: Occam 2D inversion result using both TE and TM modes for 5 profiles.

The study area resistivity distribution corresponds very well to the conceptual model of a high-enthalpy geothermal system. The up-flow area is a zone in the reservoir where the fluid flow is predominantly vertical and shows low vertical gradient temperature distribution with depth. Above the up-flow zone, the conductive clay cap is often elevated near the surface because of the relative increase in higher resistivity minerals in the mixed layer with temperature (Munoz, 2014).

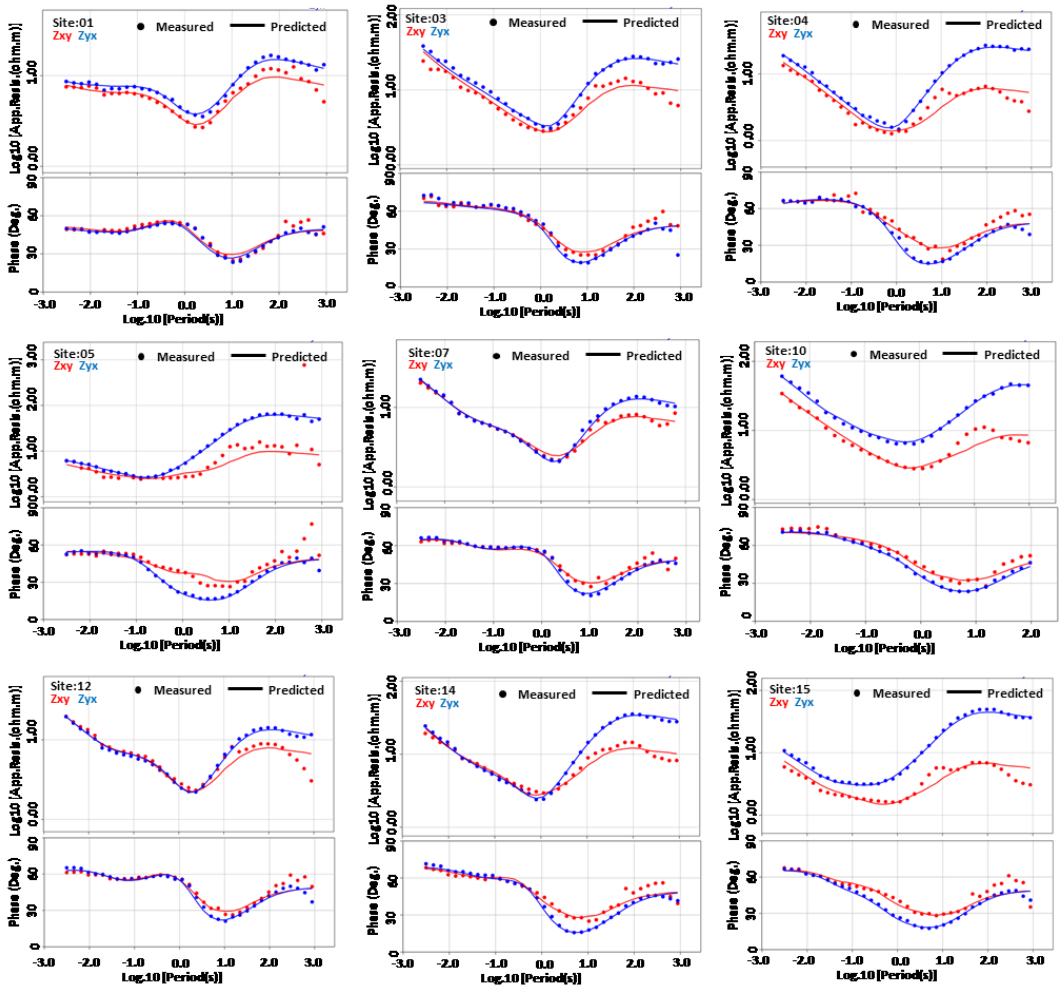

Figure 8: The 3D inversion curve fitness of selected sites from each profile. The dotted lines show the measured and the solid lines show the calculated apparent resistivity and phase.

The high resistive up-flow zone starts 800 m depth and this high resistive located in the southwestern part of the MT stations near Shalla lake, where geothermal manifestations are located. Probably this is the indication of faults in the depth. Further study is recommended in this study area to get a plausible result. The MT result of Shalla-Abayat geothermal site has a similar trend to the Langano-Aluto geothermal field.

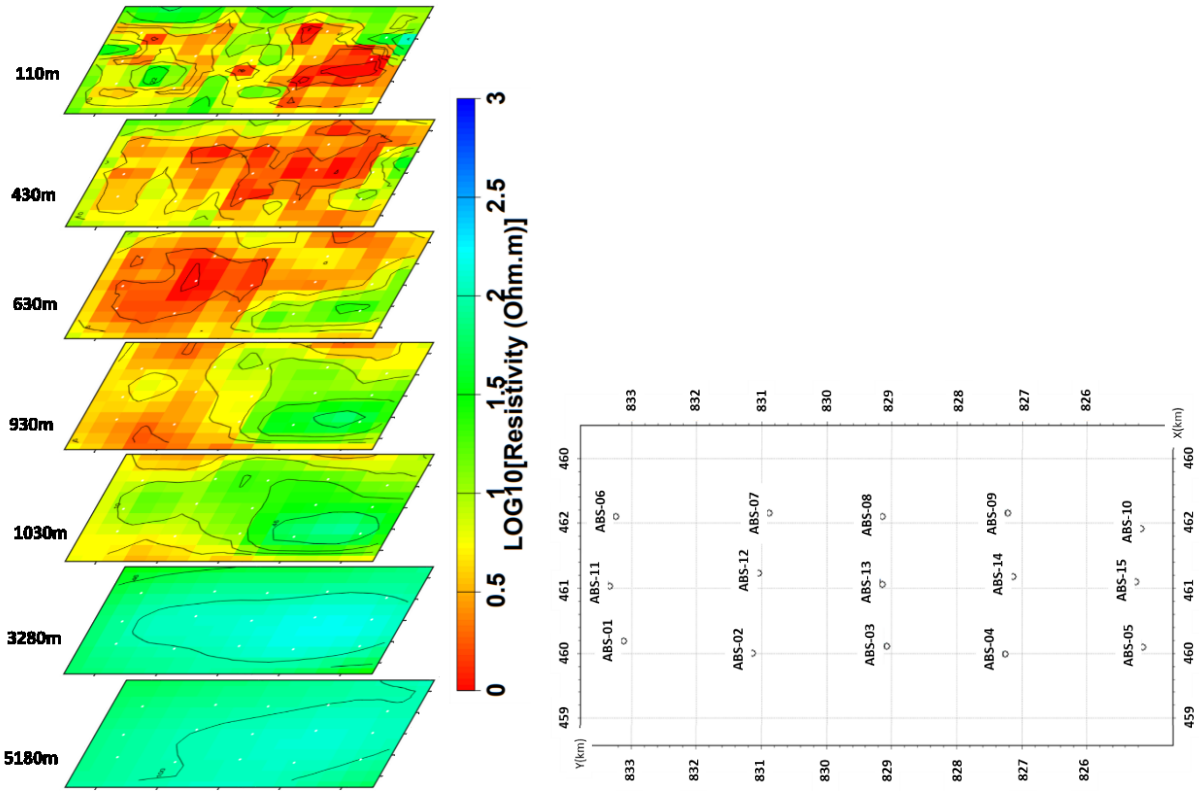

Figure 9: The horizontal resistivity distribution mapped at different depths starting from 110 to 5,180 m after 3D inversion. The white dots show the horizontal location of MT stations (left) and the location of MT data (right).

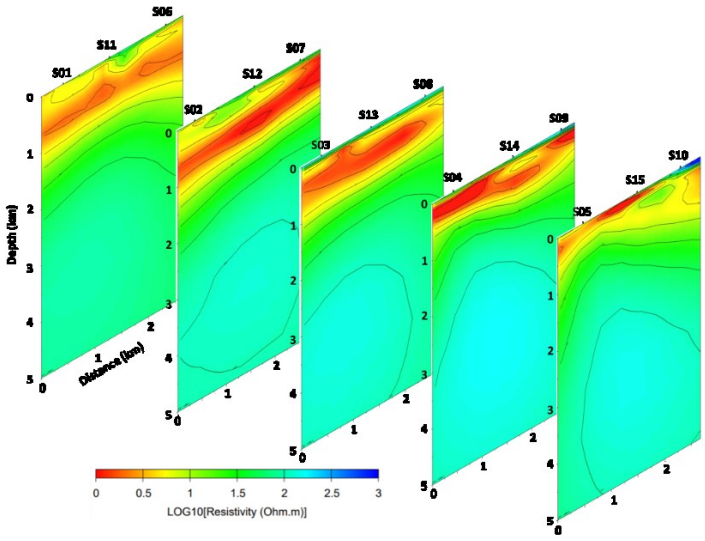

Figure 10: The 2D resistivity profiles obtained from the 3D inversion process.

5. CONCLUSION

MT data analysis of the Shalla-Abayata geothermal field reveals the dimensionality of the subsurface, indicating 2D\1D character up to 1 s and above 300 s and 3D structures at deeper depth (between 1 – 300 s) implying the need for 3D inversion to image the

subsurface structures. The inversion resistivity model of the Shalla-Abayat geothermal field interpreted with the geological information of the area and the conceptual model of high-enthalpy geothermal systems shows a similar trend to the Aluto-Langano geothermal field. The inversion resistivity model of the Shalla-Abayat geothermal field was developed using Occam for 2D and ModEM inversion code for 3D. The main resistivity structures identified using 2D and 3D inversion are: a thin high resistivity layer (80 Ωm) at shallow depth, a conductive layer underneath the high resistive zone with resistivity values below 10 Ωm, and a high resistivity region at deeper depths with resistivity values (> 80 Ωm). In a high-enthalpy geothermal system, the resistivity distribution is highly dependent on the hydrothermal alteration. The shallow high resistivity layer is associated with the fresh volcanic rocks in the unaltered zone with low temperature, where the alteration is minimum. The conductive layer is related to the argillic alteration zone due to the formation of conductive alteration minerals, particularly smectite. The resistivity increases gradually at depth beneath the conductive region and is associated with the formation of high-temperature alteration minerals, particularly chlorite and epidote in the propylitic alteration region at high temperature. The result has similar trend with Aluto-Langano geothermal field.

REFERENCES

Bahr, K., 1988: Interpretation of the magnetotelluric impedance tensor: regional induction and local telluric distortion, J. Geophys., **62**, 119–127.

Bibby, H. M., Caldwell, T.G., and Brown, C., 2005: Determinable and non-determinable parameters of galvanic distortion in magnetotellurics, Geophys. J. Int., **163**, 915–930.

Caldwell, T.G., Bibby, H.M., Brown, C., 2004. The magnetotelluric phase tensor. Geophys. J. Int., **158**, 457–469.

Chave, A.D., Jones, A.G., 2012. The Magnetotelluric Method: Theory and Practice. edn, Vol., **pp**. Pages. Cambridge University Press.

Constable. S. C. Parker, K. L. and Constable. C. G. 1987, Occam's inversion a practical algorithm for generating smooth models from EM sounding data. Geophysics, **52**, 289-300.

Cumming, W., 2009. Geothermal resource conceptual models using surface exploration data, in Proceedings, Thirty-Fourth Workshop on Geothermal Reservoir Engineering, Stanford University, Stanford, CA.

ELC-Electroconsult. (2015). Geothermal Surface Exploration in Aluto-Langano, Ethiopia. Milan, Italy, ELC Electroconsult, Report.

Egbert G. D. (1997), Robust multiple-station magnetotelluric data processing. Geophys. J. Int., **130**, 475–496, doi:10.1111/j.1365-246X.1997.tb05663.x.

Egbert, G.D., Kelbert, A., 2012. Computational recipes for electromagnetic inverse problems. Geophys. J. Int., **189**, 251–267.

Flóvenz, O., E. Spangenberg, J. Kulenkampff, K. Árnason, R. Karlsdóttir, and E. Huenges (2005), The role of electrical interface conduction in geothermal exploration, in Proceedings World Geothermal Congress 2005, Antalya, Turkey.

Gebregzabher, Z. (1986). Hydrothermal alteration minerals in Aluto Langano geothermal wells, Ethiopia, Geothermics, **15**, 735–740.

Gianelli, G., and Teklemariam, M. (1993). Water-rock interaction processes in the AlutoLangano geothermal field (Ethiopia), J. Volcanol. Geotherm. Res., **56**, 429–445.

Hamilton, M. P., Jones, A. J., Evans, R. L., Evans, S., Fourie, C. J. S., Garcia, X., …the SAMTEX MT Team. (2006). Electrical anisotropy of South African lithosphere compared with seismic anisotropy from shear-wave splitting analyses. Physics of the Earth and Planetary Interiors, **158**, 226–239. doi: 10.1016/j.pepi.2006.03.027

Kazmin, V.; Berhe, S.M. (1978): Geological map of Nazreth Sheet, Scale 1:250,000, Geological Survey of Ethiopia, Addis Ababa.

Kazmin, V. (1975): Explanation of the geological map of Ethiopia. Bulletin number one. Geological Survey of Ethiopia, Addis Ababa.

Kurtz, T., Gloaguen, R., Ebinger, C., Casey, M., Abebe, B. (2007). Deformation distribution and type in the Main Ethiopian Rift (MER): A remote sensing study.

Mohr, P.A., (1967). Major volcano-tectonic lineament in the Ethiopian Rift System. Nature, **213**, 664-665.

Munoz, G. (2014). Exploring for geothermal resources with electromagnetic methods, Surv. Geophys., **35**, 101–122.

Parkinson, W.D., 1959. Direction of rapid geomagnetic fluctuations. Geophys. J. R. Astron. Soc., **2**, 1-14.

Pellerin, L., Johnston, J. M., & Hohman, G. W. (1996). A Numerical Evaluation of Electromagnetic Methods in Geothermal Exploration. *Geophysics* , 121-130.

Saibi, H., Aboud, E. & Ehara, S., 2012. Analysis and interpretation of gravity data from the Aluto-Langano geothermal field of Ethiopia, Acta Geophys., **60**(2), 318–336.

Smirnov, M.Yu., 2003. Magnetotelluric data processing with a robust statistical procedure having a high breakdown point, Geophys. J. Int., **152**, 1–7.

Smirnov, M.Y. and Pedersen, L.B., 2009. Magnetotelluric measurements across SorgenfreiTornquist zone in southern Sweden and Denmark, Geophys. J. Int., **176**, 443–456.

Swift, C.M., 1967: A magnetotelluric investigation of electrical conductivity anomaly in the southwestern United States, PhD thesis, Massachusetts Institute of Technology, Cambridge, MA.

Teklemariam, M., Battaglia, S., Gianelli, G. & Ruggieri, G., 1996. Hydrothermal alteration in the Aluto-Langano geothermal field, Ethiopia, *Geothermics,* **25**(6), 679–702.

Tietze, K., Ritter, O., 2013. Three-dimensional magnetotelluric inversion in practice the electrical conductivity structure of the San Andreas Fault in Central California. Geophys. J. Int., **195**, 130–147.

Vozoff, K., 1972. The magnetotelluric method in the exploration of sedimentary basins. Geophysics, Soc. of Expl. Geophys., **37**, 98-141.

Wiese, H., 1962. Geomagnetische Tiefentellurik, Teil 2, Die Streichrichtung der Untergrundstrukturen des elektrischen Winderstandes, ersclossen aus geomagnetischen Variationen, Geofis. Pura. Appl., **52**, 83-103.